Role of the Transition Dipole Amplitude and Phase on the Generation of Odd and Even High-Order Harmonics in Crystals

Shicheng Jiang,[1,2] Jigen Chen,[2,3] Hui Wei,[2] Chao Yu,[1] Ruifeng Lu,[1,4,*] and C. D. Lin[2,†]

[1]*Department of Applied Physics, Nanjing University of Science and Technology, Nanjing 210094, People's Republic of China*
[2]*J. R. Macdonald Laboratory, Department of Physics, Kansas State University, Manhattan, Kansas 66506, USA*
[3]*Department of Physics, Taizhou University, Taizhou 318000, People's Republic of China*
[4]*State Key Laboratory of Molecular Reaction Dynamics, Dalian Institute of Chemical Physics, Chinese Academy of Sciences, Dalian 116023, People's Republic of China*

Since the first observation of odd and even high-order harmonics generated from ZnO crystals in 2011, the dependence of the harmonic yields on the orientation of the laser polarization with respect to the crystal axis has never been properly interpreted. This failure has been traced to the lack of a correct account of the phase of the transition dipole moment between the valence band and the conduction band. Using a simple one-dimensional two-band model, here we demonstrate that the observed odd harmonics is directly related to the orientation dependence of the magnitude of the transition dipole, while even harmonics is directly related to the phase of the transition dipole. Our result points out the essential role of the complex transition dipole moment in understanding harmonic generation from solids that has long been overlooked so far.

High-order harmonic generation (HHG) resulting from the interaction of an intense laser field with atomic or molecular gases has led to the emergence of attosecond physics and the rapid advance in ultrafast science in the past decade. HHG from a crystalline solid came along much later, not until the first observation in 2011 on ZnO [1]. Since then, HHG from many solids, including ZnO [1–5], MgO [6–8], SiO_2 [9–11], GaSe [12–14], MoS_2 [15], graphene [16,17], and rare-gas solids of Ar and Kr [18], has been reported. Like gas-phase HHG before it, harmonics from solids can be used to generate isolated attosecond pulses, but with a more compact design since it requires much lower driving laser intensities, typically a few TW/cm^2 or less. At the same time, like in atoms and molecules, HHG from solids offers opportunities for probing the structure of solids. Indeed, it has been touted that harmonics from solids can be used to reconstruct the electronic band structure [4,19] and atomic orbitals inside the crystal [6] using all-optical measurements. However, such optimism is premature since much is still unknown about HHG in solids. Experiments using driving lasers from visible to multi-THz waves each point to different generation mechanisms [1,3,5,9,10,12].

Because of the complexity of solids, it may be too naive to expect that a single mechanism can interpret high harmonic generation from all kinds of crystals. In this Letter, we go back to the basics and ask whether harmonics generated from the simplest solids can be accurately calculated. These are solids that have the simplest band structure, for example, the ZnO that was studied in 2011 [1], in particular, the harmonic yields versus the

polarization direction of the laser. These earlier experimental data have been reproduced in another recent measurement [2]. The choice of ZnO is appropriate since in the (11-20) plane where the harmonics were studied, the valence and the first conduction bands are well separated from all the higher conduction bands; thus a simple two-band model may be enough [5].

Before proceeding let us see what we know about ZnO. In Fig. 1(a), we show the wurtzite ZnO crystal in real space. The (11-20) plane is indicated by the light blue color (gray). The XYZ axes are also shown. In Figs. 1(b) and 1(c), the arrangement of Zn and O atoms on the (11-20) plane in real space, the unit cell, and the corresponding reciprocal space are displayed. On this plane, the crystal axis is along the Z axis, and the polarization angle θ of the laser is defined with respect to the crystal axis. Figure 1(d) shows the band structure along the Γ-M axis. The valence band and the first two conduction bands are marked in color. Figure 1(e) shows the magnitude of the transition dipole coupling between each pair of the three bands indicated.

The orientation-dependent harmonics obtained in Ref. [2] are displayed in Fig. 2(a). In this experiment, the authors used a 3.8 μm midinfrared laser. Their data look quite similar to the earlier ones obtained by Ghimire *et al.* [1], where the driving laser wavelength is 3.25 μm.

A quick glance at the experimental harmonic spectra in Fig. 2(a) reveals that both even and odd harmonics appear at all angles except for $\theta = 90°$, where only odd harmonics appear. In particular, even harmonics show up quite clearly near $\theta = 0°$ and 180°. [The "irregularity" for "harmonics" near the tenth order was known to be due to band
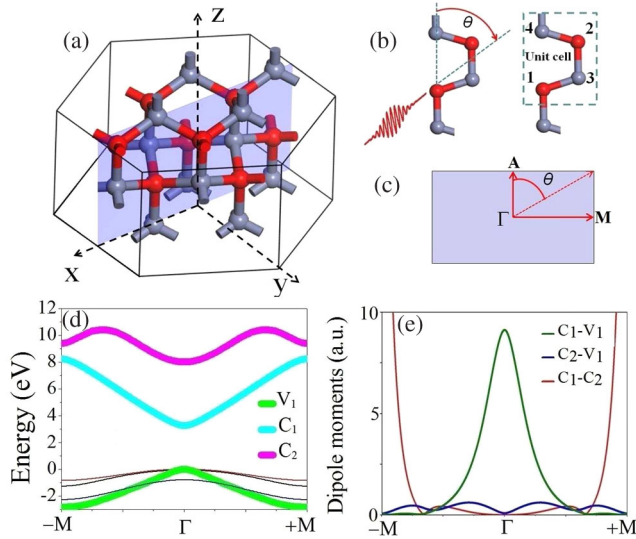
FIG. 1. (a) The crystal structure of wurtzite ZnO and the definition of the XYZ axes. The (11-20) plane is indicated by light blue color. (b) The arrangement of atoms in real space on the (11-20) plane, where O and Zn atoms are shown as red and gray balls, respectively. The unit cell and laser polarization are indicated. (c) The corresponding $k_y = 0$ plane in the reciprocal space where high symmetry **k** points are $\Gamma = (0.0, 0.0, 0.0)$, $A = (0.0, 0.0, 0.5)$, and $M = (0.5, 0.0, 0.0)$. The crystal axis is defined to be the Z axis, and the orientation angle θ is between the crystal axis and the axis of the laser polarization which lies on the (11-20) plane. (d) Band structure of ZnO. The valence band and the two lowest conduction bands are highlighted. (e) The magnitude of the transition dipole between each pair of bands considered.
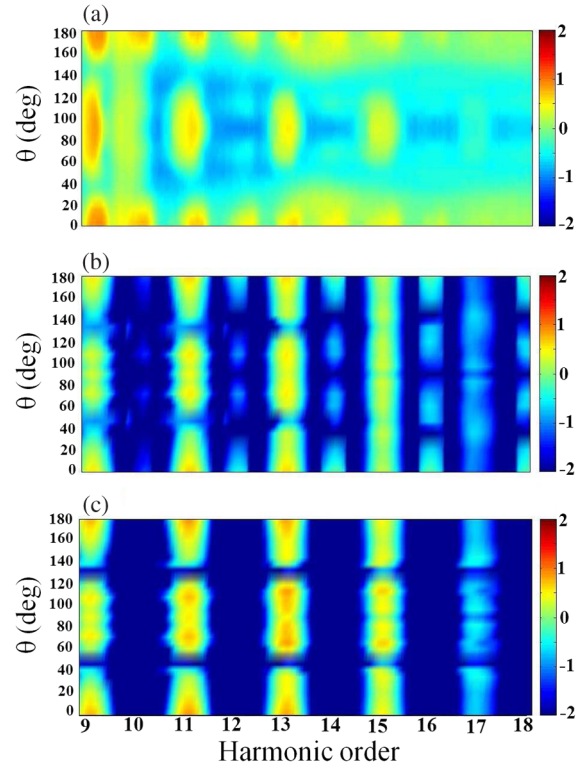

FIG. 2. (a) Orientation-dependent HHG spectra, redrawn from the experimental data in Ref. [2]. (b) Spectra calculated from the present theory. (c) Spectra calculated from the present theory but artificially removing the phase of the transition dipole between the valence and conduction bands. The efficiency of the harmonic spectra has been normalized to the 11th-order harmonic. Parameters of the lasers used are given in the text.

fluorescence (band gap is 3.3 eV) so it will not be considered further.] Such a difference in the angular dependence can be easily understood based on symmetry, by taking examples from harmonics generated in gas-phase atoms and molecules. In atoms, the target has intrinsic inversion symmetry; thus only odd harmonics exist. Consider a molecule that is fixed in space; if the molecule does not have inversion symmetry, then even harmonics would coexist with odd harmonics. Such rules should apply to solids as well. From Fig. 1(b), clearly reflection symmetry occurs when $\theta = 90°$; thus only odd harmonics appear. Away from this direction, the inversion symmetry is broken; thus even harmonics are expected, as seen in the experiment.

Oddly enough, such a self-evident prediction has not been reproduced in theoretical calculations. Previous modeling on the existence of even harmonics relies on the introduction of a second harmonic in addition to the fundamental driving laser [19]; i.e. it relies on the asymmetry of the electric field of the driving laser. In other theoretical works, the absence of even harmonics near 0° and 180° was not addressed; see Refs. [20,21]. In Refs. [12,22], it was argued that even harmonics would appear only when multiple bands are included in the calculation.

Why are the obvious results that can be deduced from symmetry alone not reproduced even qualitatively in all of these theoretical calculations? Clearly, if the calculation employs an approximation that violates symmetry, then symmetry-imposed predictions would no longer hold. As shown in our recent paper [23], the transition dipole moment is intrinsically a complex number when the system does not possess proper symmetry. In most theoretical calculations so far, it has been a common practice to neglect the phase of the transition dipole which leads automatically to the disappearance of even harmonics.

It is important to note that the band energies and transition dipole like Figs. 1(d) and 1(e) are available from most commercial codes like the Vienna *ab initio* simulation package (VASP). These codes do not provide the phase of the transition dipole. Thus the phases are simply ignored or obtained only near the Γ point using simple approximations. In these codes, the band energies are calculated at each fixed crystal momentum **k** independently by some diagonalization procedure; thus the relative phase of eigenfunctions between neighboring **k** vectors is not determined, nor is the transition dipole phase (TDP).

In this Letter, we take into account the TDP and employ the familiar semiconductor Bloch equations (SBEs) method

within the simplest 1D two-band model to calculate the angle-dependent high-order harmonics from ZnO. The results are shown in Fig. 2(b), which are to be compared to Fig. 2(a) from the experiment of Ref. [2]. One can see the agreement between the two-band model and the experiment is quite good. Even harmonics appear at angles away from $\theta = 90°$ as expected. We did try a three-band calculation, and the results are essentially the same (the difference is <1%). This is expected if one looks at the dipole moment shown in Fig. 1(e). Coupling from the valence band to the C_1 conduction band is large near the Γ point, but not near the M points. Direct coupling of the valence band with the C_2 conduction band is very small. In Fig. 2(c) we also show the two-band SBEs calculations but setting the TDP to zero artificially. Clearly all the even harmonics disappear.

Having resolved the simple issues of the existence of even versus odd harmonics in ZnO, we next check whether the details of the harmonic spectra can also be explained by the present two-band model. We defer the computational details to the Supplemental Material (SM) [24], including the parameters used to run the VASP code for generating the band structure and the transition dipole shown in Figs. 1(d) and 1(e). Since we have not been able to obtain the TDP from the VASP code, we chose to calculate the TDP based on the analytical tight-binding model. For the latter, the details are also given in the SM [24], but an outline of the method is given here.

To obtain TDP we use the semiempirical tight-binding model in Ref. [25]. The Bloch-type wave function is taken to be

$$|n, b, \mathbf{k}\rangle = \frac{1}{\sqrt{N}} \sum_{\mathbf{R}} e^{[i\mathbf{k} \cdot (\mathbf{R} + \mathbf{t}_b)]} |n, b, \mathbf{R}\rangle, \qquad (1)$$

where $|n, b, \mathbf{R}\rangle$ is the wave function localized at the site $\mathbf{R} + \mathbf{t}_b$. Here, b stands for the four atoms in the unit cell as indicated in Fig. 1(b); $n = s$, p_x, p_y, or p_z are the four different atomic orbitals. The crystal eigenstates can be expanded as $|\lambda, \mathbf{k}\rangle = \sum_{n,b} C^\lambda_{n,b} |n, b, \mathbf{k}\rangle$. We will use only six atomic orbitals per unit cell, namely, 1(O): p_x, p_z; 2(O): p_x, p_z; 3(Zn): s; 4(Zn): s. We further include only the on-site integrals and the nearest-neighbor two-center integrals, thus reducing to a 6×6 Hamiltonian matrix. After the matrix is diagonalized analytically, we can obtain the $\mathbf{k}$-dependent transition dipole phases between bands λ_1 and λ_2 from Eq. (S14) in the SM [24].

Note that the transition dipole moments are obtained based on the three-dimensional (3D) wave functions; thus, the dipole moments contain $D_x(\mathbf{k})$, $D_y(\mathbf{k})$, and $D_z(\mathbf{k})$. We reduce the 3D problem to a 1D problem by projecting the 3D dipole moment onto the polarization direction of the driving laser. Once the band energies and transition dipole amplitude and phase (TDP) are calculated as described above, we solved the 1D two-band SBEs. In the experiment, the pulse duration is estimated to be 100 fs and the intensity is about 1–2 TW/cm^2, while in the theory they
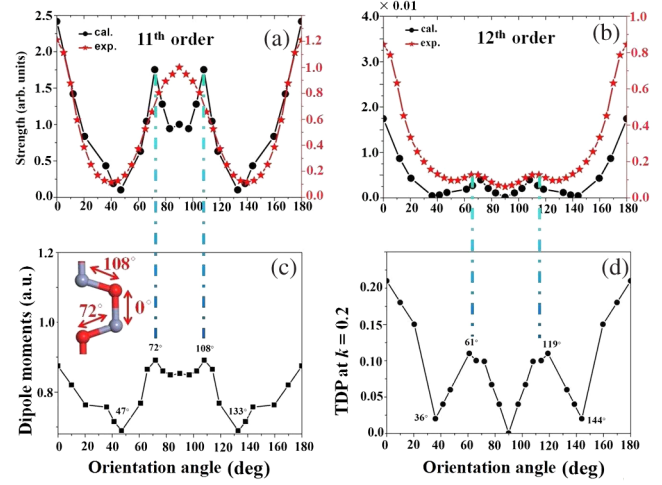

FIG. 3. (a),(b) Comparison of theoretical and experimental orientation-dependent harmonic strength of the 11th-order and the 12th-order harmonics, respectively. (c) The square of the absolute value of the transition dipole moments $\bar{D}$ versus the orientation angle of the laser polarization direction. (d) The same quantity as in (c) but multiplied by the square of the phase of the transition dipole at $k = 0.2$. See text for details.

are 65 fs and 9×10^{10} W/cm^2, respectively. Recall that the experimental intensity refers to outside the crystal and in the calculation it refers to within the crystal. The intensity for the theory was chosen such that the harmonic spectra exhibit best agreement with the experimental data.

Next we examine the details of the measured and calculated harmonic spectra. We comment that the experimental data shown in Fig. 2(a) have been replotted using the digital data provided by the authors of Ref. [2], to allow for better visualization when compared to the calculations. The fine features to be discussed below are not as clearly seen in the published data in Ref. [2], especially the weaker signals away from $\theta = 0°$ and 180°. In order to make a quantitative comparison, we define the strength P_i of the ith-order harmonic by integrating the harmonic signal from $(i - 0.5)\omega$ to $(i + 0.5)\omega$, where ω is the photon energy of the driving laser. The strengths of the 11th and 12th harmonics are then selected for comparison in Figs. 3(a) and 3(b), respectively.

We first focus on the 11th-order odd harmonic shown in Fig. 3(a). Theory shows maxima at 0°, 72°, 108°, and 180°, and minima at 47° and 133° approximately. The results agree well with experimental data except for angles close to 90° where experiment has only one peak located at 90°. Since a large dipole transition matrix element would lead to higher ionization probability of an electron from the valence band, we explore the angle-dependent harmonic yields versus the square of the absolute values of the transition dipole moment $\bar{D}$ around the Γ point. The latter are shown in Fig. 3(c). Here, $\bar{D}$ is defined as $\bar{D} = \int_{-0.05}^{+0.05} D(K) dk$. One can clearly see the nearly identical angular modulations between Figs. 3(a) and 3(c). This is a clear illustration that the angle-dependent

harmonic yield is directly related to the square of absolute value of the angle-dependent transition dipole element.

We next focus on the angle dependence of the 12th-order even harmonic; see Fig. 3(b). The peaks at 0° and 180° are similar to the odd harmonics. A more obvious valley is observed at 90° for both the experimental data and the calculated results. The disappearance of even harmonics at 90° is of course due to the reflection symmetry of the crystal along this direction where the TDP is always zero (or a constant). Clearly, one would examine how the harmonics are related to the angle-dependent transition dipole phase. In our previous paper [23] [near Eq. (38)] we demonstrated that the efficiency of even harmonics depends on $\sin^2(\Delta\beta)$, where $\Delta\beta = |\beta_r - \beta_i|$, i.e., the difference of the TDP between the subcycle excitation time and the recombination time. Assuming that electrons are excited from the Γ point where the TDP is set to zero, then $\Delta\beta = |\beta_r|$. Since $|\beta_r|$ is small, we further replace its sine function by the phase itself. Thus, in Fig. 3(d), we plot the angular dependence of $|D|^2||\beta_r|^2$ to compare with Fig. 3(b). The angular dependence from Fig. 3(d) matches the theoretical HHG spectra in Fig. 3(b), which is shifted only slightly from the experimental data. Comparing Figs. 3(c) and 3(d), the phase factor $|\beta_r|^2$ is 2 orders smaller. This is also reflected by the fact that even harmonics is about 2 orders smaller than odd harmonics. We comment that the TDP is given at $k = 0.2$ in Fig. 3(d), but its trend does not change for other k points.

A few additional comments on Fig. 3 are in order. First, the inset in Fig. 3(c) shows the bond angles in ZnO. Note that the angles indicated happen to also be where the dipole moments are also at the maximum. So this is an example that angle-dependent harmonic signals can be directly related to the arrangement of atoms in the crystal. Qualitatively, the observed orientation-dependent harmonics yields observed in MgO was also interpreted in terms of bond angles [6], but actual calculations in MgO show the maxima of the transition dipole do not always lie along the direction of the interatomic axis. Since the reciprocal space and real space are not independent, it is not surprising that interpretation in terms of real space parameters may work, but the more fundamental quantity in describing harmonic generation is the transition dipole. Clearly, even harmonics cannot be explained in terms of real space since the phase is involved. Finally, in the SM [24], we show additional data for harmonics from the 13th to 16th. One can conclude that all the odd harmonics have the same angular dependence, and all the even harmonics have the same angular dependence.

In Figs. 2(b), 3(a), and 3(b), the present 1D model contains only parallel components of the harmonics. We can add the contribution of the perpendicular components calculated using the linearly coupled excitations (LCE) model [14]. A description of this model and the new results are shown to compare even better with experimental data; see SM [24].
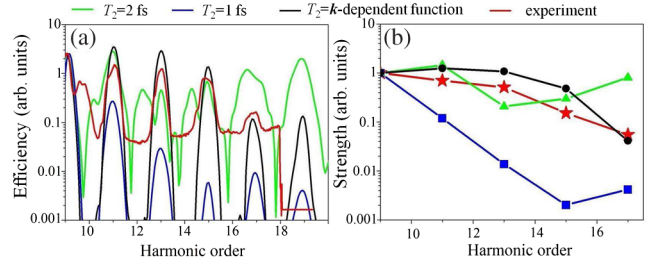

FIG. 4. (a) The dependence of the calculated harmonics on the dephasing time and the comparison with experimental data. The colored lines on the top indicate the different dephasing time and the color for the experimental data. (b) Comparison of the strength of the harmonics versus the dephasing time.

In the SBEs model, a phenomenological dephasing time T_2 is often introduced to account for the loss of coherence due to the interaction of the excited electron with the crystal medium. The parameter T_2 will modify the relative strength and the "coherence" of the harmonics generated. Figure 4 shows how the harmonic yields at $\theta = 90°$ versus different values of T_2. To obtain narrow harmonic peaks as observed in the experiment, as shown in Fig. 4(a), $T_2 = 1$ fs is the best. However, the calculated higher-order harmonics then drop much faster than the experiment. If $T_2 = 2$ fs is used, then each harmonic becomes very broad, but the relative peak heights become closer to the observation. Figure 4(b) shows the quantitative comparison. Since the scattering of the laser-driven electron with the crystal is expected to depend on the momentum of the electron, we introduce a k-dependent T_2. We found that if we choose T_2 to have a bell-shaped form, $T_2(k) = 1 + 1/[1 + \exp(100|k| - 5)]$, then the calculated harmonic yields as well as the sharpness of the harmonics would best agree with the data. This bell-shaped function gives $T_2 = 2$ fs at $k = 0$. It drops quickly to 1.5 fs at $|k| = 0.05$ a.u. For larger $|k|$ away from the Γ point, it reduces to 1 fs quickly. Note that the $\mathbf{k}$-dependent dephasing time $T_2(\mathbf{k})$ has been discussed and mentioned in Refs. [26–29].

In conclusion, we have demonstrated that a one-dimensional two-band SBEs model can nicely explain the observed orientation-dependent high-order harmonic spectra for ZnO reported in Refs. [1,2]. The keys to the success are the accurate band energies and the transition dipole between the two bands. We demonstrated that the correct phase of the transition dipole is essential to explain the even harmonics. The phase appears to have been overlooked in most of the previous theoretical treatment of harmonics in solids. Our result is reminiscent of HHG in gas-phase molecules where it was established in the quantitative rescattering theory [30,31] that an accurate angle-dependent complex transition dipole is essential for the correct description of harmonics in molecules. The success of the two-band model in ZnO would pave the way for extending the theory to more complex multiple-band models for other solids, but only if the TDPs are correctly calculated.

Looking ahead, much remains to be done. It is imperative to find an efficient computational method to calculate the phase of the transition dipole that is not available in today's commercial crystal structure packages. Next, it is desirable to extend the 1D SBE calculation to 3D such that the polarization of the harmonics [14] can also be explored. In addition, the dephasing time has been introduced in the SBE method to bypass the need of carrying out propagation of harmonics in the medium. A critical test of this procedure may benefit from the measurement of the phase of the harmonics.

*rflu@njust.edu.cn
†cdlin@phys.ksu.edu

[1] S. Ghimire, A. D. DiChiara, E. Sistrunk, P. Agostini, L. F. DiMauro, and D. A. Reis, Nat. Phys. **7**, 138 (2011).
[2] S. Gholam-Mirzaei, J. Beetar, and M. Chini, Appl. Phys. Lett. **110**, 061101 (2017).
[3] G. Vampa, T. J. Hammond, N. Thiré, B. E. Schmidt, F. Légaré, C. R. McDonald, T. Brabec, and P. B. Corkum, Nature (London) **522**, 462 (2015).
[4] G. Vampa, T. J. Hammond, N. Thiré, B. E. Schmidt, F. Légaré, C. R. McDonald, T. Brabec, D. D. Klug, and P. B. Corkum, Phys. Rev. Lett. **115**, 193603 (2015).
[5] Z. Wang, H. Park, Y. H. Lai, J. Xu, C. I. Blaga, F. Yang, P. Agostini, and L. F. DiMauro, Nat. Commun. **8**, 1686 (2017).
[6] Y. S. You, D. A. Reis, and S. Ghimire, Nat. Phys. **13**, 345 (2017).
[7] S. Ghimire, J. Phys. B **47**, 204030 (2014).
[8] Y. S. You et al., Opt. Lett. **42**, 1816 (2017).
[9] T. T. Luu, M. Garg, S. Yu. Kruchinin, A. Moulet, M. Th. Hassan, and E. Goulielmakis, Nature (London) **521**, 498 (2015).
[10] M. Garg, M. Zhan, T. T. Luu, H. Lakhotia, T. Klostermann, A. Guggenmos, and E. Goulielmakis, Nature (London) **538**, 359 (2016).
[11] Y. S. You, Y. Yin, Y. Wu, A. Chew, X. Ren, F. Zhuang, S. Gholam-Mirzaei, M. Chini, Z. Chang, and S. Ghimire, Nat. Commun. **8**, 724 (2017).
[12] O. Schubert et al., Nat. Photonics **8**, 119 (2014).
[13] M. Hohenleutner, F. Langer, O. Schubert, M. Knorr, U. Huttner, S. W. Koch, M. Kira, and R. Huber, Nature (London) **523**, 572 (2015).
[14] F. Langer, M. Hohenleutner, U. Huttner, S. W. Koch, M. Kira, and R. Huber, Nat. Photonics **11**, 227 (2017).
[15] H. Liu, Y. Li, Y. S. You, S. Ghimire, T. F. Heinz, and D. A. Reis, Nat. Phys. **13**, 262 (2016).
[16] N. Yoshikawa, T. Tamaya, and K. Tanaka, Science **356**, 736 (2017).
[17] M. Taucer et al., Phys. Rev. B **96**, 195420 (2017).
[18] G. Ndabashimiye, S. Ghimire, M. Wu, D. A. Browne, K. J. Schafer, M. B. Gaarde, and D. A. Reis, Nature (London) **534**, 520 (2016).
[19] A. A. Lanin, E. A. Stepanov, A. B. Fedotov, and A. M. Zheltikov, Optica **4**, 516 (2017).
[20] C. D. Liu, Y. H. Zheng, Z. N. Zeng, and R. X. Li, Phys. Rev. A **93**, 043806 (2016).
[21] E. N. Osika, A. Chacón, L. Ortmann, N. Suárez, J. A. Pérez-Hernández, B. Szafran, M. F. Ciappina, F. Sols, A. S. Landsman, and M. Lewenstein, Phys. Rev. X **7**, 021017 (2017).
[22] T. T. Luu and H. J. Wörner, Phys. Rev. B **94**, 115164 (2016).
[23] S. C. Jiang, H. Wei, J. G. Chen, C. Yu, R. F. Lu, and C. D. Lin, Phys. Rev. A **96**, 053850 (2017).
[24] See Supplemental Material at http://link.aps.org/supplemental/10.1103/PhysRevLett.120.253201 for the expression of the multi-band semiconductor Block Equations, the description and parameters for the band structure calculations and the tight-binding model. Additional results for higher-order harmonics and the inclusion of perpendicularly polarized harmonics using the LCE model are also given in the SM.
[25] A. Kobayashi, O. F. Sankey, S. M. Volz, and J. D. Dow, Phys. Rev. B **28**, 935 (1983).
[26] T. Takagahara, Quantum Coherence, Correlation and Decoherence in Semiconductor Nanostructures (Academic Press, London, 2003), Chap. 2.
[27] F. Langer et al., Nature (London) **533**, 225 (2016).
[28] I. Floss, C. Lemell, G. Wachter, V. Smejkal, S. A. Sato, X. M. Tong, K. Yabana, and J. Burgdorfer, Phys. Rev. A **97**, 011401 (2018).
[29] C. R. McDonald, A. B. Taher, and T. Brabec, J. Opt. **19**, 114005 (2017).
[30] T. Morishita, A.-T. Le, Z. Chen, and C. D. Lin, Phys. Rev. Lett. **100**, 013903 (2008).
[31] A.-T. Le, R. R. Lucchese, S. Tonzani, T. Morishita, and C. D. Lin, Phys. Rev. A **80**, 013401 (2009).